

# Charting and unzipping the surface layer of *Corynebacterium glutamicum* with the atomic force microscope

Simon Scheuring,<sup>1,2</sup> Henning Stahlberg,<sup>1</sup>  
Mohamed Chami,<sup>1,2</sup> Christine Houssin,<sup>3</sup>  
Jean-Louis Rigaud<sup>2</sup> and Andreas Engel<sup>1\*</sup>

<sup>1</sup>M. E. Müller Institute for Microscopy at the Biozentrum, University of Basel, Klingelbergstrasse 70, CH-4056 Basel, Switzerland.

<sup>2</sup>Institut Curie, UMR-CNRS 168 and LRC-CEA 8, 11 rue Pierre et Marie Curie, 75231 Paris Cedex 05, France.

<sup>3</sup>Laboratoire de Biologie Moléculaire des *Corynebactéries*, URA 1354 CNRS, Université de Paris-Sud, 91405 Orsay, France.

## Summary

**Bacterial surface layers (S-layers) are extracellular protein networks that act as molecular sieves and protect a large variety of archaea and bacteria from hostile environments. Atomic force microscopy (AFM) was used to assess the S-layer of *Corynebacterium glutamicum* formed of PS2 proteins that assemble into hexameric complexes within a hexagonal lattice. Native and trypsin-treated S-layers were studied. Using the AFM stylus as a nanodissector, native arrays that adsorbed to mica as double layers were separated. All surfaces of native and protease-digested S-layers were imaged at better than 1 nm lateral resolution. Difference maps of the topographies of native and proteolysed samples revealed the location of the cleaved C-terminal fragment and the sidedness of the S-layer. Because the corrugation depths determined from images of both sides span the total thickness of the S-layer, a three-dimensional reconstruction of the S-layer could be calculated. Lattice defects visualized at 1 nm resolution revealed the molecular boundaries of PS2 proteins. The combination of AFM imaging and single molecule force spectroscopy allowed the mechanical properties of the *Corynebacterium glutamicum* S-layer to be examined. The results provide a basis for understanding the amazing stability of this protective bacterial surface coat.**

## Introduction

Surface layers (S-layers) represent the outermost cell wall layer of many Bacteria and Archaea (Baumeister *et al.*, 1989; Sleytr *et al.*, 1993; Sleytr, 1997; Engelhardt and Peters, 1998), and are regular two-dimensional protein networks (Baumeister *et al.*, 1988). These layers withstand non-physiological pH, radiation, temperature, proteolysis, pressure and detergent treatment (Baumeister *et al.*, 1986; Chami *et al.*, 1997; Engelhardt and Peters, 1998), thus protecting the cell from such hostile factors. Moreover, they serve as molecular sieves as well as in phage recognition (Baumeister and Hegerl, 1986; Smith and Agre, 1991; Sleytr *et al.*, 1993; 1997; Wang *et al.*, 1993).

PS2 is the protein that forms the S-layer of *Corynebacterium glutamicum* (Peyret *et al.*, 1993; Bahl *et al.*, 1997; Chami *et al.*, 1997). The layer was shown to be stable in 3% SDS at temperatures up to 60°C (Chami *et al.*, 1997). Using SDS-PAGE, the native monomer reveals an apparent molecular weight (MW) of 63 kDa (Chami *et al.*, 1997). The C-terminus of the protein contains a stretch of 21 hydrophobic amino acids. Proteolysis of the S-layer removed the C-terminus, resulting in a protein with an apparent MW of 56 kDa (Chami *et al.*, 1997) and leading to detachment of the S-layer from the cell. In agreement, bacteria expressing the shortened PS2 protein could not assemble the S-layer, but released the protein into the medium (Chami *et al.*, 1997), indicating that the C-terminus functions in S-layer/cell wall attachment.

Atomic force microscopy (AFM; Binnig *et al.*, 1986) has become a powerful tool for observing proteins in their native environment (Engel and Müller, 2000). AFM is capable of imaging protein surfaces at subnanometre resolution in their native environment (Schabert *et al.*, 1995; Czajkowsky and Shao, 1998; Scheuring *et al.*, 1999; Seelert *et al.*, 2000). A combination of AFM imaging and proteolysis experiments allows protein domain positions and sidedness to be assigned (Scheuring *et al.*, 1999; 2001; Fotiadis *et al.*, 2000). Furthermore, the AFM tip was used to measure the forces involved in unfolding single proteins (Rief *et al.*, 1997; 2000; Oberhauser *et al.*, 1998). Recently, imaging and single molecule force spectroscopy have been combined (Müller *et al.*, 1999a; Oesterhelt *et al.*, 2000).

Accepted 3 January, 2002. \*For correspondence. E-mail andreas.engel@unibas.ch; Tel. (+41) 61 267 22 61; Fax (+41) 61 267 21 09.

	Native S-layer	Digested S-layer
Unit cell dimensions	a = b = 16.0 ± 0.2 nm (n = 10) $\gamma = 60 \pm 1^\circ$ (n = 10)	a = b = 16.0 ± 0.2 nm (n = 10) $\gamma = 60 \pm 1^\circ$ (n = 10)
Layer thickness	4.6 ± 0.1 nm (n = 20)	4.1 ± 0.1 nm (n = 20)
Maximal surface indentation		
Flower-shaped surface	3.5 nm (n = 20)	3.0 nm (n = 20)
Triangular surface	2.0 nm (n = 20)	2.0 nm (n = 20)
Imaging resolution		
Flower-shaped surface	1.0 nm <sup>a</sup>	1.0 nm <sup>a</sup>
Triangular surface	1.0 nm <sup>a</sup>	1.0 nm <sup>a</sup>
Adsorption on mica	Double-layer stacks	Single layer
Assignment of the		
Flower-shaped surface	Inner surface	Inner surface
Triangular surface	Outer surface	Outer surface
Hydrophilicity/hydrophobicity		
Flower-shaped surface	Hydrophobic	Hydrophilic
Triangular surface	Hydrophilic	Hydrophilic
Unzipping		
Flower-shaped surface	Possible	Not possible
Triangular surface	Not possible	Not possible

**Table 1.** Characteristics of the S-layer of *C. glutamicum*.

a. Diffraction spots are found corresponding to higher resolution (see Fig. 3).

We have used AFM to investigate the S-layer of *C. glutamicum*. Native and trypsin-treated samples were tightly adsorbed to the mica AFM support and imaged under native conditions. The adsorption behaviour of the two samples differs strikingly, indicating that one surface of the native S-layer is not hydrophilic and tends to stack. The AFM tip was used to dissect such double-layered assemblies (Hoh *et al.*, 1991; Schabert *et al.*, 1995;

Fotiadis *et al.*, 2000). High-resolution topographs ( $\approx 1.0$  nm) revealed two different surface types, one flower shaped and one triangular. The S-layer was found to have a thickness of 4.6 nm for the native and 4.1 nm for the proteolysed sample, both with unit cell dimensions of a = b = 16 nm,  $\gamma = 60^\circ$ . Section analysis of images recorded with a very sharp AFM tip showed that the height information from both surfaces spanned the total height

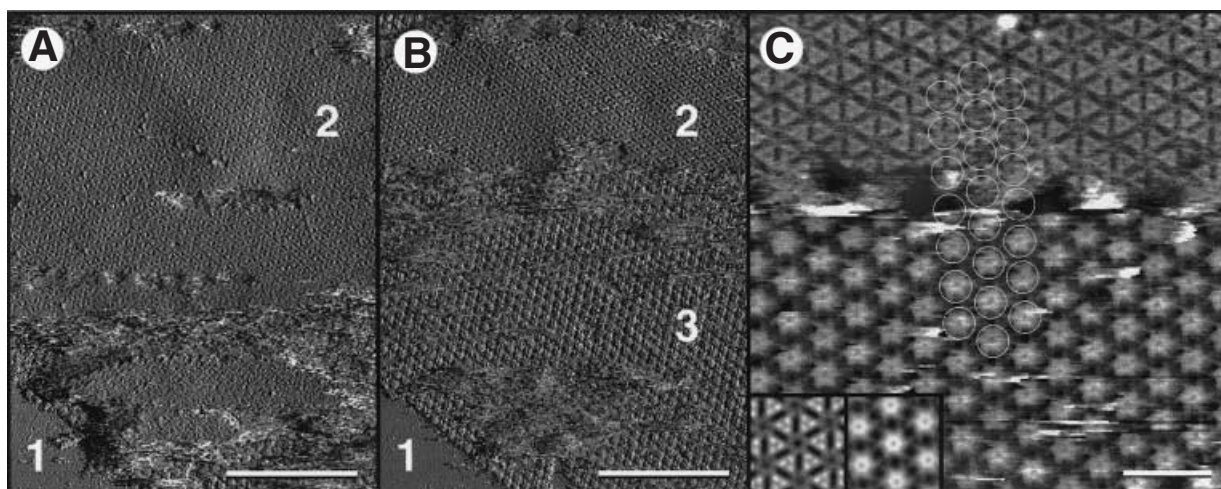


**Fig. 1.** Overview images of the double-stacked native S-layer.

A. Deflection image of a double-stacked S-layer. The smooth surface (bottom left, labelled 1) is the mica AFM support. The surface with triangular appearance is exposed to the tip (labelled 2). The flower-shaped surface can only be seen on the edges of the patch (scale bar = 100 nm; full grey scale: 1 nm).

B. Deflection image of the same region imaged 5 min later. The top layer (triangular appearance) has been partially scratched to expose the flower-shaped surface underneath (labelled 3) (scale bar = 100 nm; full grey scale: 1 nm).

C. The scratching of the top layer (top of the image) can be conducted in a controlled manner by applying  $\approx 600$  pN (bottom of the image). Insets show averages of the top and bottom part of the image. Circles indicate the stacking contact regions (i.e. the hexameric cores) between the two layers (scale bar = 50 nm; full grey scale: 5 nm).

of the S-layer; hence, the reconstruction of a three-dimensional model from AFM topographs was possible for the first time. Thus, imaging of defects allowed the molecular organization of the protein network to be revealed. Force spectroscopic measurements provided information about the mechanical properties of the S-layer and reflect the molecular architecture of the assembly.

## Results

### Atomic force microscopy imaging

Native and trypsin-treated S-layers of *C. glutamicum* were imaged by AFM in physiological buffer. The proteolytic treatment removed an  $\approx 8$  kDa fragment of the C-terminus, changing the apparent MW of the monomer from  $\approx 64$  kDa to  $\approx 56$  kDa (Chami *et al.*, 1997). Both forms, the native and digested S-layer, adsorbed tightly to mica and were imaged after washing in 10 mM Tris-HCl, pH 7.5, 250 mM KCl. The thickness of the S-layers was determined from medium magnification images ( $\approx 500$  nm  $\times$   $\approx 500$  nm scan area) to  $4.6 \pm 0.1$  nm ( $n = 20$ ) and  $4.1 \pm 0.1$  nm ( $n = 20$ ) for the native and digested samples (Table 1). Native S-layers adsorbed to the mica surface as double or multilayers (Fig. 1, Table 1). They exposed a surface with a triangular appearance when imaged at forces applied to the AFM tip of  $\approx 100$  pN (Fig. 1A). Scanning the same area with a force of  $\approx 600$  pN applied to the stylus removed the top layer in a controlled manner (Fig. 1B). The layer underneath exposed a strikingly different flower-shaped surface structure (Fig. 1B). Topographs of dissection border regions recorded at higher magnification revealed that the layers stacked with their sixfold symmetry centres in register (Fig. 1C).

In contrast to the native layers, the digested S-layers adsorbed mainly to the mica surface as single layers in random orientation exposing each surface with equal probability (Fig. 2A). Section analysis on the flower-shaped surface displayed on the left part of the image (Fig. 2A, lines 1 and 2; Table 1) revealed strong indentations of 3.0 nm (Fig. 2B, sections 1 and 2). The triangular surface on the right part of the image (Fig. 2A, lines 3 and 4) is less corrugated, 2.0 nm (Fig. 2B, sections 3 and 4; Table 1).

High-resolution AFM topographs (Fig. 3) revealed the native and digested S-layer to have unit cell dimensions of  $a = b = 16.0$  nm  $\pm 0.2$  nm and  $\gamma = 60 \pm 1^\circ$  (Table 1). Both surfaces of the native sample, the flower-shaped (Fig. 3A and E) and the triangular (Fig. 3H and L), could be imaged at a lateral resolution better than 1 nm, as judged from calculated diffraction patterns (Fig. 3B and I). Images of the flower-shaped (Fig. 3C and F) and the triangular (Fig. 3J and M) surfaces of the digested sample also diffracted

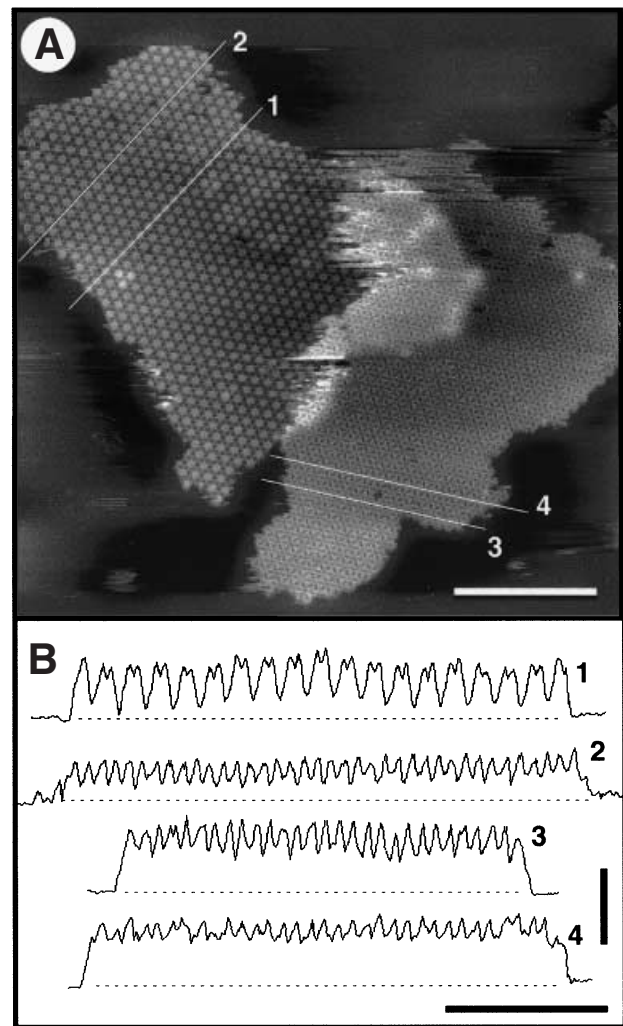


**Fig. 2.** Overview image and section analysis of the trypsin-treated S-layer.

A. Height image of two single patches adsorbed to the mica surface. The flower-shaped surface (left) and the triangular-shaped surface (right) adsorb equally well to the mica support (scale bar = 200 nm; full grey scale: 5 nm).

B. Section analysis along the correspondingly numbered lines in (A). Line 1 crossing the flower-shaped surface; line 2 analysing the connection arms between the flower-shaped surfaces; line 3 crossing the triangular surface; line 4 analysing the backside of the flower-shaped surface in between the triangles [lateral scale bar = 100 nm; vertical scale bar = 5 nm; baseline corrected (dashed lines)].

better than 1 nm resolution (Fig. 3D and K). In order to locate the cleaved hydrophobic C-terminus (Chami *et al.*, 1997), difference maps were calculated between corresponding surfaces of the native and the protease-treated samples. The difference maps revealed a well-defined density on the flower-shaped surface (Fig. 3G) and only minor differences on the triangular surface (Fig. 3N). This is in agreement with the observations that (i) the native sample stacks into double layers with their flower-shaped surfaces interacting (Fig. 1); (ii) the native flower-shaped

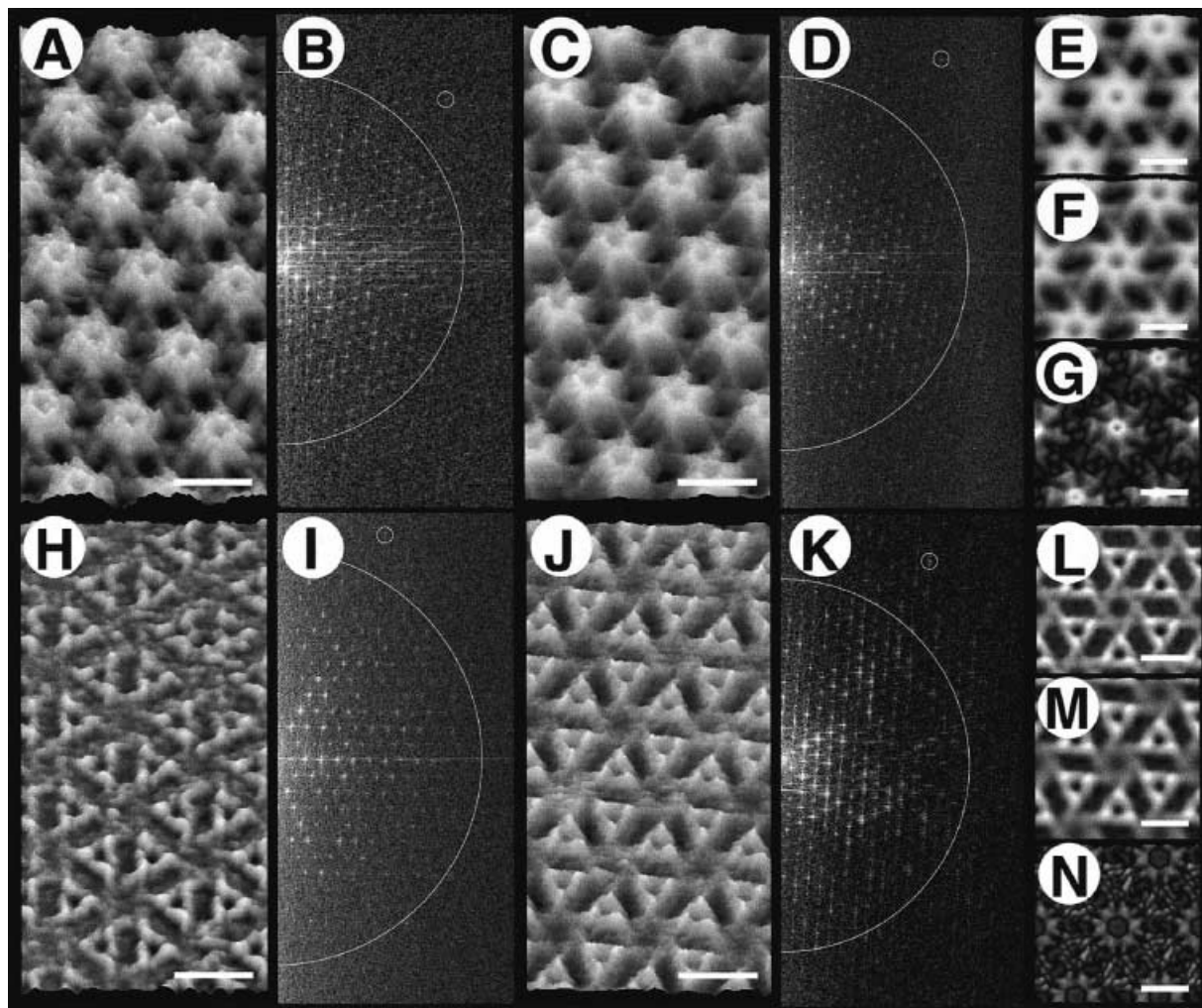


**Fig. 3.** High-resolution AFM topographs of native and digested S-layer recorded in buffer solution (10 mM Tris-HCl, pH 7.5, 250 mM KCl) lead to identification of the flower-shaped surface as cell wall connected and the triangular-shaped surface as extracellular. All images displayed 15° tilted.

- A. Flower-shaped surface of the native S-layer (scale bar = 15 nm; full grey scale: 3.5 nm).  
 B. Calculated power spectrum of the full image shown in (A). Large circle:  $1 \text{ nm}^{-1}$ , small circle: diffraction spot at subnanometre resolution.  
 C. Flower-shaped surface of the digested S-layer (scale bar = 15 nm; full grey scale: 3.0 nm).  
 D. Calculated power spectrum of the full image shown in (C). Large circle:  $1 \text{ nm}^{-1}$ , small circle: diffraction spot at subnanometre resolution.  
 E. Sixfold symmetrized cross-correlation average of image (A) (scale bar = 5 nm; full grey scale: 3.5 nm).  
 F. Sixfold symmetrized cross-correlation average of image (C) (scale bar = 5 nm; full grey scale 3.5 nm).  
 G. Sixfold symmetrized difference map calculated from averages (E) and (F) (scale bar = 5 nm; full grey scale: 1 nm).  
 H. Triangular-shaped surface of the native S-layer (scale bar = 15 nm; full grey scale: 2.0 nm).  
 I. Calculated power spectrum of the full image shown in (H). Large circle:  $1 \text{ nm}^{-1}$ , small circle: diffraction spot at subnanometre resolution.  
 J. Triangular-shaped surface of the digested S-layer (scale bar = 15 nm; full grey scale: 2.0 nm).  
 K. Calculated power spectrum of the full image shown in (I). Large circle:  $1 \text{ nm}^{-1}$ , small circle: diffraction spot at subnanometre resolution.  
 L. Sixfold symmetrized cross-correlation average of image (H) (scale bar = 5 nm; full grey scale 2.0 nm).  
 M. Sixfold symmetrized cross-correlation average of image (J) (scale bar = 5 nm; full grey scale 2.0 nm).  
 N. Sixfold symmetrized difference map calculated from averages (L) and (M) (scale bar = 5 nm; full grey scale: 0.4 nm).

surface does not adsorb to the hydrophilic mica (Fig. 1, Table 1); (iii) the digested sample adsorbs with both surfaces equally to the hydrophilic mica surface (Fig. 2); and (iv) the digested sample has a reduced layer thickness of 0.5 nm (Table 1). A maximal density difference ( $\leq 1.0 \text{ nm}$ ) is found close to the sixfold symmetry centre of the flower-shaped surface corresponding to a ring-shaped structure

(Fig. 3E), whereas the density differences on the triangular surface are widely distributed with values  $\leq 0.4 \text{ nm}$  (Fig. 3J). According to the arguments above, the exposed hydrophobic flower-shaped surface (Fig. 3A) thus faces the cell wall and is probably buried into the cell wall lipid molecules (Chami *et al.*, 1997).

The strong surface corrugation of 3.5 nm observed on

## Atomic force microscopy force spectroscopy

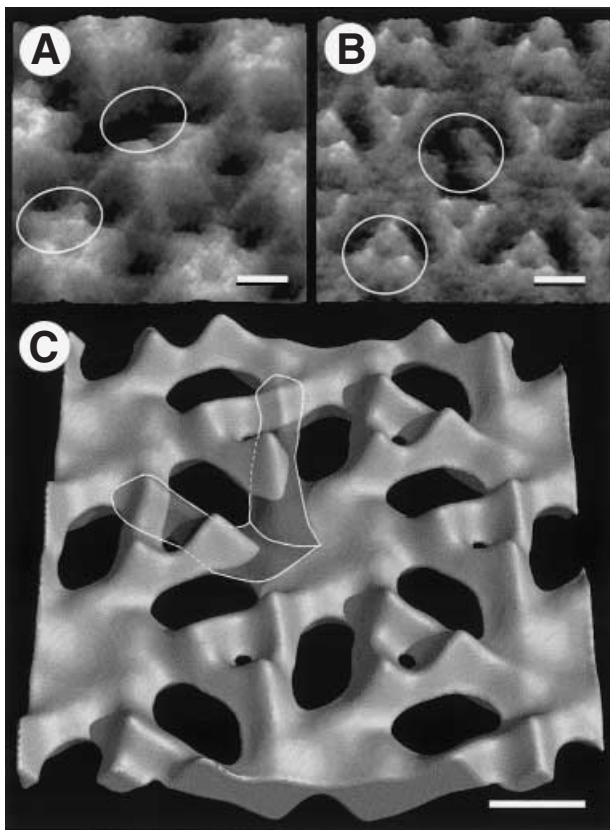


**Fig. 4.** Molecular recognition of the monomers within the S-layer protein network.  
 A. Defect of two monomers viewed from the inner flower-shaped surface. The defects allow us to identify unambiguously which arm between the hexameric symmetry centre corresponds to which monomer (scale bar = 5 nm; full grey scale: 3.5 nm).  
 B. Monomer defects viewed from the outer triangular-shaped surface leaving one arm of a triangle exposed alone (scale bar = 5 nm; full grey scale: 2.0 nm).  
 C. Three-dimensional reconstruction viewed from the outer surface. Two units are shaded, and putative monomer boundaries are outlined indicating the arm-over-arm connectivity of the protein S-layer network (scale bars = 5 nm).  
 Circles in (A) and (B) mark differences between native cores and cores exposing molecular defects.

the flower-shaped surface and 2.0 nm on the triangular surface of the native sample and, correspondingly, 3.0 nm and 2.0 nm of the digested sample, span the total layer thickness of 4.6 nm and 4.1 nm (Fig. 2B, Table 1). Hence, a three-dimensional reconstruction of the layer could be calculated (Fig. 4C).

Imaging single molecule defects viewed from both sides (Fig. 4A and B) allowed us to delineate the molecular boundaries of the S-layer units (Fig. 4C). The monomers of each hexameric core extend outwards to form triangular connections between neighbouring cores. Within these triangles, three monomers from three neighbouring cores form arm-over-arm protein-protein contacts (Fig. 4C).

The flower-shaped, hydrophobic inner surface of the native S-layer adhered to the AFM tip and promoted assessment of the mechanical stability of the protein layer network using the AFM tip by unzipping single molecules (Müller *et al.*, 1999a). A large number of force-distance curves were acquired, classified and evaluated using a new force curve classification procedure (see *Experimental procedures*). Different types of force-distance curves were observed (Fig. 5). In general, the force curves acquired on the flower-shaped inner surface of the native S-layer reveal a repulsive interaction with a standard deviation below 10 pN ( $n = 53$ ) (Fig. 5A). However, attractive interactions between the AFM tip and the protein network, as shown in Fig. 5B with an adhesion peak of  $70 \pm 25$  pN ( $n = 30$ ), occurred in  $\approx 5\%$  of the tip sample approaches. Furthermore, three different types of force-distance curves were reproducibly acquired with one, two or three strong rupture peaks of  $250 \pm 60$  pN ( $n = 33$ ),  $280 \pm 40$  pN ( $n = 21$ ) and  $260 \pm 60$  pN ( $n = 12$ ) with periodicity of 21 nm (Fig. 5, Table 2). These strong rupture peaks are interspersed by faint peaks of  $80 \pm 35$  pN ( $n = 35$ ),  $70 \pm 25$  pN ( $n = 21$ ) and  $60 \pm 25$  pN ( $n = 12$ ), also with a periodicity of 21 nm, 12 nm before each strong rupture peak (indicated by the arrows in Figs 5 and 6, Table 2; see also Fig. 7). The three types of force-distance curves also feature an ill-defined peak of  $70 \pm 40$  pN ( $n = 35$ ) close to the lift-off point (indicated by the asterisks in Figs 5 and 6).

The concomitant removal of subunits from the S-layer ensemble was documented by AFM imaging before and after force curve acquisition (Fig. 6; see *Experimental procedures*). The control topographs of the same regions acquired after the force measurements show that subunits were removed in pairs up to a complete hexamer, compatible with the simultaneously acquired force curves (Fig. 6). A model is proposed to explain this dimer-like unzipping behaviour of the hexameric cores of the of *C. glutamicum* S-layer (Fig. 7, see *Discussion*).

## Discussion

The S-layer of *C. glutamicum* is a hexagonal protein array with extraordinary properties that indicate its protective function (Chami *et al.*, 1995). Among the wide variety of S-layers described (Sleytr and Messner, 1983; 1988; Baumeister *et al.*, 1988; Engelhardt and Peters, 1998), the well-characterized hexagonal packed intermediate (HPI) layer of *Deinococcus radiodurans* exhibits most striking similarities, although the two species are located on different branches of the phylogenetic tree. Similar to the HPI layer (Baumeister *et al.*, 1986; Karrasch *et al.*, 1994; Müller *et al.*, 1996), the native S-layers of *C.*

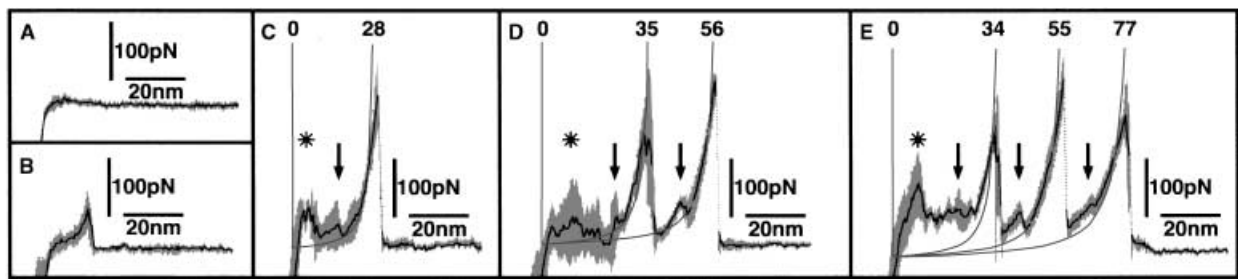


**Fig. 5.** Averages (see *Experimental procedures*) of force–distance curves recorded on the inner surface of the S-layer of *C. glutamicum*.

A. Average of 10 representatives out of a cluster of 53 repulsive force–distance curves.

B. Average of 10 representatives out of a cluster of 30 adhesive force–distance curves (adhesive force:  $70 \pm 25$  pN).

C. Average of seven representatives out of a cluster of 12 force–distance curves with one strong rupture peak.

D. Average of four representatives out of a cluster of nine force–distance curves with two strong rupture peaks.

E. Average of five representatives out of a cluster of 12 force–distance curves with three strong rupture peaks.

All average force–distance curves are cantilever deflection corrected. SD values at each point are displayed as a grey shadow on both sides of the curve. The rupture curves were fitted using the WLC model.

*glutamicum* adsorb to mica in physiological buffer (Müller *et al.*, 1997), stack into oppositely oriented double layers and adsorb with only one surface to hydrophilic mica (Fig. 1). This suggests one of the two surfaces to be hydrophobic, compatible with its interaction with the outer membrane in the case of *D. radiodurans* and with the complex lipid-containing cell envelope in the case of *C. glutamicum* (Chami *et al.*, 1997; Puech *et al.*, 2001). In particular, we show that the C-terminal domain forms an exposed hydrophobic ring structure about the sixfold symmetry axis that mediates anchoring and might form a pore (Fig. 3), in agreement with the definition of S-layer pores (Engelhardt and Peters, 1998). Both S-layers show a hexagonal packing of the monomers with similar lattice dimensions [HPI: 18 nm (Baumeister *et al.*, 1986); *C. glutamicum* S-layer: 16 nm; this work], but differ in their thickness, 7.0 nm for the HPI layer (Engel *et al.*, 1982; Baumeister *et al.*, 1986; Müller *et al.*, 1996) and 4.6 nm for the *C. glutamicum* S-layer (this work). These differences are compatible with the different MWs of the units of 104 kDa (*D. radiodurans*; Peters and Baumeister, 1986) and 50 kDa (*C. glutamicum*; Chami *et al.*, 1997).

The large unit cell dimension and the relatively loose packing of the S-layer units within the protein network

allowed sharp AFM tips to penetrate between proteins almost down to the mica surface (Fig. 2B, line 1). The surface corrugation of both sides was determined to 3.5 nm and 2.0 nm. Because the sum, 5.5 nm, is larger than the total thickness of 4.6 nm of the native S-layer, the available height information allowed a three-dimensional model of the S-layer to be calculated (Fig. 4C). Lattice defects imaged at subnanometre resolution revealed the molecular boundaries and thus the interaction between the S-layer units. Monomers form hexameric cores, which interact with their arms with two other units each.

To acquire high-resolution topographs the tip sample interaction was minimized by electrostatic balancing (Müller *et al.*, 1999b). In contrast, the tip was pressed onto the sample with 500–800 pN to achieve strong adhesion of the hydrophobic C-terminus (Müller *et al.*, 1999a). Five types of force–distance curves were reproducibly acquired on the inner surface of the native S-layer (Fig. 5). Imaging before and after force–distance curve acquisition allowed us to correlate force spectroscopic measurements with changes of surface topography. Curves with strong rupture events (Figs 5C–E and 6C, F and I) document the unzipping of protein and their removal from the S-layer assembly (Fig. 6A, B, D, E, G and H). After each

	Rupture force	<i>n</i>	Rupture length from lift-off <sup>a</sup>	Rupture length from last protomer <sup>a</sup>
Adhesion	$70 \pm 25$ pN	10	12 nm	
Breaking 1–6	$70 \pm 40$ pN	33	0–12 nm	
Protomer 1	$80 \pm 35$ pN	33	22 nm	10 nm <sup>b</sup>
Protomer 2	$250 \pm 60$ pN	33	35 nm	13 nm
Protomer 3	$70 \pm 25$ pN	21	44 nm	9 nm
Protomer 4	$280 \pm 40$ pN	21	56 nm	12 nm
Protomer 5	$60 \pm 25$ pN	12	65 nm	9 nm
Protomer 6	$260 \pm 60$ pN	12	77 nm	12 nm

a. Derived from curve fits (see Fig. 5; *Experimental procedures*).

b. Measured from the end of protomer 1–6 breaking force peak.

**Table 2.** Unzipping statistics of the S-layer of *C. glutamicum*.

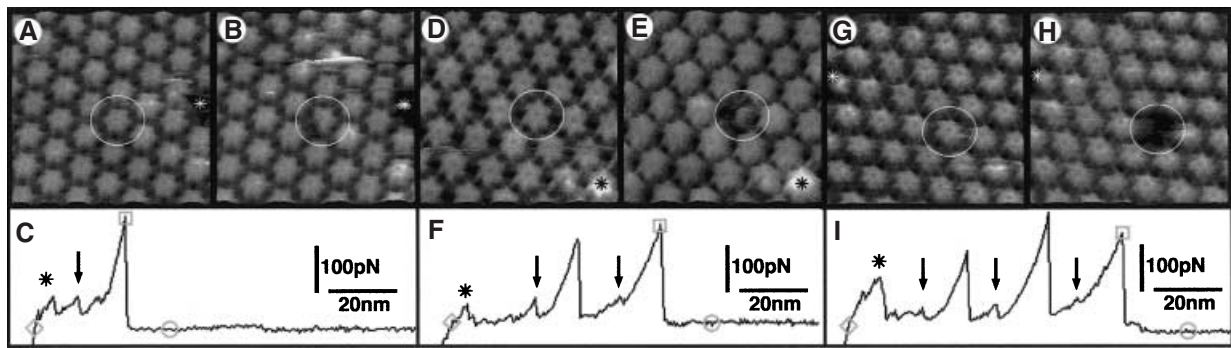


**Fig. 6.** Structural correlation of force–distance curve measurements on the S-layer of *C. glutamicum*.

A. Image before and after (B) unzipping of two protomers out of a hexameric core.

C. Force–distance curve corresponding to the change in the surface structure as shown in (A) and (B).

D. Image before and after (E) unzipping of four protomers out of a hexameric core.

F. Force–distance curve corresponding to the change in the surface structure as shown in (D) and (E).

G. Image before and after (H) unzipping of a full hexameric core.

I. Force–distance curve corresponding to the change in the surface structure as shown in (G) and (H).

All images have dimensions of 100 nm square; asterisks indicate lattice defects, which allow alignment of the sets of two images. Circles in the force–distance curves indicate the zero-force baseline; the diamonds indicate the putative lift-off point; and the squares indicate the last rupture peak used for force–distance curve alignment (see *Experimental procedures*). Arrows indicate the faint rupture peaks of the odd-numbered protomers, and the asterisks the odd defined breaking rupture between protomer 1 and 6 (see *Discussion*).

rupture event, a single scan at low magnification and thus high scan speed ensured acceptable image quality and the correct position of the subsequent high-magnification scan (see *Experimental procedures*). Rupture events indicated by the force–distance curve were always confirmed by the missing subunits in post-zipping high-resolution topographs.

Interestingly, the unzipping of a total hexameric core reveals three major rupture peaks ( $\approx 270$  pN) interspersed by three faint peaks ( $\approx 70$  pN). This is in contrast to the six rupture peaks ( $\approx 300$  pN) measured for the removal of one hexameric core of the S-layers of *D. radiodurans*. This striking difference in the force curves reflects the different packing arrangements of the two hexagonal protein lattices. Although *D. radiodurans* HPI-layer proteins assemble into hexameric cores with each protein making one additional connection with one protomer of another core, the *C. glutamicum* S-layer proteins form hexameric cores with each protein being connected to two protomers from two other cores (Fig. 7). Saxton and Baumeister (1986) have established a classification scheme considering the assembly of S-layer proteins into massive cores (M) and connecting structures (C). Accordingly, *D. radiodurans* features an  $M_6C_2$  layer and *C. glutamicum* an  $M_6C_3$  layer. The six almost equal force peaks observed upon unzipping the HPI layer are explained by strong interaction forces between subunits within the core and weaker forces (i.e. 300 pN) between slender arms interacting at C2 sites (Müller *et al.*, 1999a). Hence, each peak documents the rupture of a single bond between the core being unzipped and one of its six adjacent cores. In contrast, in the  $M_6C_3$  protein assembly of the *C. glutami-*

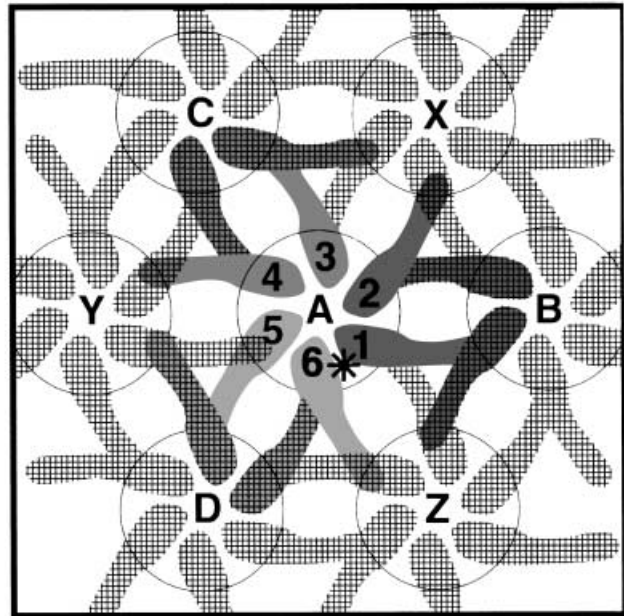


**Fig. 7.** Model for the unzipping of the S-layer of *C. glutamicum* (see also *Discussion*).

The central hexameric core (A) is circularly numbered with an arbitrary beginning, displaying a putative unzipping sequence.

The dimer-like unzipping behaviour is explained by the  $M_6C_3$  packing (Saxton and Baumeister, 1986). Subunits 1 and 2 can act co-operatively with two subunits (shaded grid pattern) of the core (B). Units 3 and 4 are not connected with (B), but have co-operative interaction with two units of core (C), 5 and 6 with (D). In case unzipping starts with unit 2 cores, (X) (Y), and (Z) are responsible for the dimer-like behaviour. The asterisks represent the breaking region between units (6) and (1) at the beginning of the unzipping.

*cum* S-layer (Fig. 7), unit (1) of core (A) is connected to one unit of core (B), while unit (2) of (A) is also connected with (B), but in a different conformation. Assuming that the tip is firmly attached to unit (A1), the withdrawal forces will first destabilize core (B) and, as (A2) is also connected to this core, (A1) and (A2) exhibit co-operativity, as documented by force curves with a small and a large peak. This process may be repeated until a complete hexamer is removed, explaining the dimer-like unzipping behaviour of the  $M_6C_3$  protein assembly. Because the surface topographies are not compatible with a threefold symmetry of the core unit [root mean square (RMS) deviation from sixfold symmetry <2%], co-operativity between adjacent monomers resulting from interactions at the  $C_3$  centres is the best interpretation of the force spectra observed. To prove this hypothesis, atomic scale structural information is required.

Force peaks of this magnitude are found only among the most strongly interacting biomolecules. To rupture the bond between avidin and biotin, a force of 160 pN is required (Florin *et al.*, 1994). Likewise, the most strongly interacting antibody–epitope pairs reported yield rupture forces of 60 pN (Dammer *et al.*, 1996) and 244 pN (Hinterdorfer *et al.*, 1996). That similar forces are required to unzip the HPI layer or the *C. glutamicum* S-layer document the extraordinary stability of these protein networks that protect microorganisms from a hostile environment.

## Experimental procedures

### Sample preparation

The native S-layer from of *C. glutamicum* was extracted from whole cells using 1% SDS at room temperature. Digested S-layers were prepared by the addition of 5  $\mu$ g of trypsin per 1 ml of bacterial culture. Subsequently, cells were sedimented at 3000 *g*. S-layer fragments were pelleted by centrifugation at 16 000 *g* and washed three times with buffer (20 mM Tris-HCl, pH 7.5) (for more details, see Chami *et al.*, 1995; 1997).

### Atomic force microscope set-up

Imaging of native and protease-treated S-layers and force spectroscopy were performed with a commercial Nanoscope III AFM (Digital Instruments) equipped with a 162  $\mu$ m scanner (J-scanner) and oxide-sharpened  $Si_3N_4$  cantilevers with a length of 100  $\mu$ m ( $k = 0.09$  N  $m^{-1}$ ; Olympus).

### Atomic force microscopy imaging

Mica prepared as described by Schabert and Engel (1994) was used as support and freshly cleaved before every experiment using Scotch tape. To check the cleavage quality, the mica was imaged in 30–50  $\mu$ l of adsorption buffer (10 mM Tris-HCl, pH 7.5, 250 mM KCl, 50 mM  $MgCl_2$ ). Subsequently, 2  $\mu$ l of S-layer solution (0.1 mg  $ml^{-1}$ ) was injected into the

adsorption buffer drop on the mica surface. After 30 min, the sample was rinsed with 10 volumes of recording buffer (10 mM Tris-HCl, pH 7.5, 250 mM KCl). The AFM was operated in contact mode applying forces below  $\approx$  100 pN at a scan line frequency of 4–6 Hz. The sharpest tips adequate for high-resolution imaging were cleaned in 1% SDS and subsequently washed three times in distilled water.

### AFM image processing

AFM images of S-layers were processed by correlation averaging using the SEMPER image processing system (Saxton *et al.*, 1979). The three-dimensional reconstruction was calculated from high-resolution topography averages in the SPIDER software package (Frank *et al.*, 1996) and displayed with POVRAY ([www.povray.org](http://www.povray.org)).

### Atomic force microscopy force spectroscopy

Force spectroscopy measurements were conducted under imaging conditions with the AFM set-up described above. The tip was placed onto the flower-shaped inner surface of the native S-layer. A full frame image (512  $\times$  512 pixels; scan area  $\approx$  200 nm) was taken before and after force spectroscopy measurement to correlate measured force–distance curves with structural changes on the S-layer surface. In case the tip was contaminated by an unzipped protomer, an intermediate low-magnification scan at high scan speed was performed to decontaminate the tip and reposition the imaging area. The AFM stylus was approached to and retracted from the inner S-layer surface with a speed of 200 nm  $s^{-1}$ . Contact forces between tip and surface to allow efficient adhesion of PS2 molecules were typically 500–800 pN. After successful removal of S-layer protomers, the interaction area was changed. All measurements were conducted at 25°C.

### AFM force spectroscopy analysis

AFM force curves were transferred to the SEMPER image processing system (Saxton *et al.*, 1979) including all parameters required to process the curves quantitatively (piezo, photodiode and cantilever characteristics). Force–distance curves were aligned and classified automatically. In a first step, the no-contact area (average over 100 points) far away from the surface was used to align all curves to the zero-force baseline (indicated by the circles in Fig. 6C, F and I). The lift-off point from the surface in the force–distance curve was defined as the crossing point of the leftmost part of the force curve (i.e. the contact region) and the baseline (indicated by the diamonds in Fig. 6C, F and I). Rupture maxima of the force curves and their position were determined and used to classify force–distance curves by the number of peaks found and the distance of the last peak from the lift-off point (indicated by the squares in Fig. 6C, F and I). In this way, up to 30 force curve clusters were assembled and scrutinized to remove curves exhibiting artifacts. SEMPER routines were then used to calculate force–distance curve averages after alignment by cross-correlation, leading to an average and a standard deviation value for each point along the force curve (Fig. 5). Force curves were corrected for cantilever deflection

at each point and fitted using the worm-like chain (WLC) model:  $F(x) = (kT/b) * [0.25 * (1-x/L)^{-2} - 0.25 + x/L]$ , where  $F(x)$  is the force at extension  $x$ ;  $k$  is the Boltzmann constant;  $b = 0.4$  nm is the persistence length; contour length  $L$  of the polypeptide chain; and  $T$  is 298 (K) (Bustamante *et al.*, 1994). Force–distance curves were never compressed or stretched during the classification and averaging process.

### Acknowledgements

The authors thank Dr Patrick Frederix for fruitful discussions. This work was supported by the Swiss National Foundation for Scientific Research (grant 31-59415.99 to A.E.), the Maurice E. Müller Foundation of Switzerland, the Centre National de la Recherche Scientifique of France and the Université Paris-Sud, France.

### References

- Bahl, H., Scholz, H., Bayan, N., Chami, M., Leblon, G., Gulik-Krzywicki, T., *et al.* (1997) Molecular biology of S-layers. *FEMS Microbiol Rev* **20**: 47–98.
- Baumeister, W., and Hegerl, R. (1986) Can S-layers make bacterial connexons? *FEMS Microbiol Lett* **36**: 119–125.
- Baumeister, W., Barth, M., Hegerl, R., Guckenberger, R., Hahn, M., and Saxton, W.O. (1986) Three-dimensional structure of the regular surface layer (HPI layer) of *Deinococcus radiodurans*. *J Mol Biol* **187**: 241–253.
- Baumeister, W., Wildhaber, I., and Engelhardt, H. (1988) Bacterial surface proteins: some structural, functional and evolutionary aspects. *Biophys Chem* **29**: 39–49.
- Baumeister, W., Wildhaber, I., and Phipps, B.M. (1989) Principles of organization in eubacterial and archebacterial surface proteins. *Can J Microbiol* **35**: 215–227.
- Binnig, G., Quate, C.F., and Gerber, C. (1986) Atomic force microscope. *Phys Rev Lett* **56**: 930–933.
- Bustamante, C., Marko, J.F., Siggia, E.D., and Smith, S. (1994) Entropic elasticity of lambda-phage DNA. *Science* **265**: 1599–1600.
- Chami, M., Bayan, N., Dedieu, J.-C., Leblon, G., Shechter, E., and Gulik-Krzywicki, T. (1995) Organization of the outer layers of the cell envelope of *Corynebacterium glutamicum*: a combined freeze-etch electron microscopy and biochemical study. *Biol Cell* **83**: 219–229.
- Chami, M., Bayan, N., Peyret, J.L., Gulik-Krzywicki, T., Leblon, G., and Shechter, E. (1997) The S-layer protein of *Corynebacterium glutamicum* is anchored to the cell wall by its C-terminal hydrophobic domain. *Mol Microbiol* **23**: 483–492.
- Czajkowsky, D.M., and Shao, Z. (1998) Submolecular resolution of single macromolecules with atomic force microscopy. *FEBS Lett* **430**: 51–54.
- Dammer, U., Hegner, M., Anselmetti, D., Wagner, P., Dreier, M., Huber, W., and Güntherodt, H.J. (1996) Specific antigen/antibody interactions measured by force microscopy. *Biophys J* **70**: 2437–2441.
- Engel, A., and Müller, D.J. (2000) Observing single biomolecules at work with the atomic force microscope. *Nature Struct Biol* **7**: 715–718.
- Engel, A., Baumeister, W., and Saxton, W. (1982) Mass mapping of a protein complex with the scanning transmission electron microscope. *Proc Natl Acad Sci USA* **79**: 4050–4054.
- Engelhardt, H., and Peters, J. (1998) Structural research on surface layers: a focus on stability, surface layer homology domains, and surface layer–cell wall interactions. *J Struct Biol* **124**: 276–302.
- Florin, E.-L., Moy, V.T., and Gaub, H.E. (1994) Adhesion forces between individual ligand–receptor pairs. *Science* **264**: 415–417.
- Fotiadis, D., Hasler, L., Müller, D.J., Stahlberg, H., Kistler, J., and Engel, A. (2000) Surface tongue-and-groove contours on lens MIP facilitate cell-to-cell adherence. *J Mol Biol* **300**: 779–789.
- Frank, J., Radermacher, M., Penczek, P., Zhu, J., Li, Y., Ladjadj, M., and Leith, A. (1996) SPIDER and WEB: processing and visualization of images in 3D electron microscopy and related fields. *J Struct Biol* **116**: 190–199.
- Hinterdorfer, P., Baumgartner, W., Gruber, H.J., Schilcher, K., and Schindler, H. (1996) Detection and localization of individual antibody–antigen recognition events by atomic force microscopy. *Proc Natl Acad Sci USA* **93**: 3477–3481.
- Hoh, J.H., Lal, R., John, S.A., Revel, J.-P., and Arnsdorf, M.F. (1991) Atomic force microscopy and dissection of gap junctions. *Science* **253**: 1405–1408.
- Karrasch, S., Hegerl, R., Hoh, J., Baumeister, W., and Engel, A. (1994) Atomic force microscopy produces faithful high-resolution images of protein surfaces in an aqueous environment. *Proc Natl Acad Sci USA* **91**: 836–838.
- Müller, D.J., Baumeister, W., and Engel, A. (1996) Conformational change of the hexagonally packed intermediate layer of *Deinococcus radiodurans* imaged by atomic force microscopy. *J Bacteriol* **178**: 3025–3030.
- Müller, D.J., Amrein, M., and Engel, A. (1997) Adsorption of biological molecules to a solid support for scanning probe microscopy. *J Struct Biol* **119**: 172–188.
- Müller, D.J., Baumeister, W., and Engel, A. (1999a) Controlled unzipping of a bacterial surface layer with atomic force microscopy. *Proc Natl Acad Sci USA* **96**: 13170–13174.
- Müller, D.J., Fotiadis, D., Scheuring, S., Müller, S.A., and Engel, A. (1999b) Electrostatically balanced subnanometer imaging of biological specimens by atomic force microscopy. *Biophys J* **76**: 1101–1111.
- Oberhauser, A.F., Marszalek, P.E., Erickson, H.P., and Fernandez, J.M. (1998) The molecular elasticity of the extracellular matrix protein tenascin. *Nature* **393**: 181–185.
- Oesterhelt, F., Oesterhelt, D., Pfeiffer, M., Engel, A., Gaub, H.E., and Müller, D.J. (2000) Unfolding pathways of individual bacteriorhodopsins. *Science* **288**: 143–146.
- Peters, J., and Baumeister, W. (1986) Molecular cloning, expression, and characterization of the gene for the surface (HPI)-layer protein of *Deinococcus radiodurans* in *Escherichia coli*. *J Bacteriol* **167**: 1048–1054.
- Peyret, J.L., Bayan, N., Joliff, G., Gulik-Krzywicki, T., Mathieu, L., Shechter, E., and Leblon, G. (1993) Characterization of the cspB gene encoding PS2, an ordered surface-layer protein in *Corynebacterium glutamicum*. *Mol Microbiol* **9**: 97–109.
- Puech, V., Chami, M., Lemassu, A., Laneelle, M.-A.,

- Schiffler, B., Gounon, P., *et al.* (2001) Structure of the cell envelope of corynebacteria: importance of non-covalently bound lipids in the formation of the cell wall permeability barrier and fracture plane. *Microbiology* **147**: 1365–1382.
- Rief, M., Gautel, M., Oesterhelt, F., Fernandez, J.M., and Gaub, H.E. (1997) Reversible unfolding of individual titin immunoglobulin domains by AFM. *Science* **276**: 1109–1112.
- Rief, M., Gautel, M., and Gaub, H.E. (2000) Unfolding forces of titin and fibronectin domains directly measured by AFM. *Adv Exp Med Biol* **481**: 129–136.
- Saxton, W.O., and Baumeister, W. (1986) Principles of organization in S layers. *J Mol Biol* **187**: 251–253.
- Saxton, W.O., Pitt, T.J., and Horner, M. (1979) Digital image processing: the semper system. *Ultramicroscopy* **4**: 343–354.
- Schabert, F.A., and Engel, A. (1994) Reproducible acquisition of *Escherichia coli* porin surface topographs by atomic force microscopy. *Biophys J* **67**: 2394–2403.
- Schabert, F.A., Henn, C., and Engel, A. (1995) Native *Escherichia coli* OmpF porin surfaces probed by atomic force microscopy. *Science* **268**: 92–94.
- Scheuring, S., Ringler, P., Borgina, M., Stahlberg, H., Müller, D.J., Agre, P., and Engel, A. (1999) High resolution topographs of the *Escherichia coli* waterchannel aquaporin Z. *EMBO J* **18**: 4981–4987.
- Scheuring, S., Freiss-Husson, F., Engel, A., Rigaud, J.-L., and Ranck, J.-L. (2001) High resolution topographs of the *Rubrivivax gelatinosus* light-harvesting complex 2. *EMBO J* **20**: 3029–3035.
- Seelert, H., Poetsch, A., Dencher, N.A., Engel, A., Stahlberg, H., and Müller, D.J. (2000) Proton powered turbine of a plant motor. *Nature* **405**: 418–419.
- Sleytr, U.B. (1997) Basic and applied S-layer research: an overview. *FEMS Microbiol Rev* **20**: 5–12.
- Sleytr, U.B., and Messner, P. (1983) Crystalline surface layers on bacteria. *Annu Rev Microbiol* **37**: 311–339.
- Sleytr, U.B., and Messner, P. (1988) Crystalline surface layers in prokaryotes. *J Bacteriol* **170**: 2891–2897.
- Sleytr, U.B., Messner, P., Pum, D., and Sára, M. (1993) Crystalline bacterial cell surface layers: general principles and application potential. *J Appl Bacteriol Symp Suppl* **74**: 21S–32S.
- Sleytr, U.B., Bayley, H., Sara, M., Breitwieser, A., Kupcu, S., Mader, C., *et al.* (1997) Applications of S-layers. *FEMS Microbiol Rev* **20**: 151–175.
- Smith, B.L., and Agre, P. (1991) Erythrocyte Mr 28,000 transmembrane protein exists as a multisubunit oligomer similar to channel proteins. *J Biol Chem* **266**: 6407–6415.
- Wang, E., Garcia, M.M., Blake, M.S., Pei, Z., and Blaser, M.J. (1993) Shift in S-layer protein expression responsible for antigenic variation in *Campylobacter fetus*. *J Bacteriol* **175**: 4979–4984.